

4.1 Radiation Sources

The main objective of the ID effort is to perform R&D to improve ID performance and meet new user needs for radiation with special characteristics and to handle major breakdowns of operating IDs.

A strategy for ID development was conceived in the early years of the APS project: to develop and build a universal ID that could provide radiation over a large energy range, 5 to 25 keV, without compromising the record high brilliance expected from a third-generation source. In order to achieve this goal, state-of-the-art techniques and equipment needed to be developed.

High brilliance could only be delivered if the magnetics of the ID were properly designed and were accurately tuned after fabrication. The precise magnetic tuning, in turn, required an advanced measurement system.

The wide energy range to be covered by the ID dictated a high peak magnetic field that could be varied in a precise and controllable manner. This led to the need for sophisticated controls and innovative vacuum systems with small vertical apertures.

Finally, experimental verification of the design and fabrication of the ID required a set of diagnostic equipment capable of measuring the absolute spectral flux under the conditions of record high x-ray power density. The results of these measurements would need to be compared to theoretical calculations.

The progress in realizing these goals is recounted in the remainder of this section of the report.

4.1.1 Magnetic Measurements and Tuning of IDs

It is imperative that APS users be provided with a stable x-ray beam. Nothing must perturb the x-ray beam by more than a few percent of its size and angular divergence. However, the x-ray beam can be perturbed if there is a change in the steering of the positron beam through an undulator. A small change in the positron beam steering could cause a large change in the position of the photon beam at the user's experiment due to the long distance between the source and the experiment. If the magnetic field of an ID is not well tuned, changes in the ID gap could cause changes in the positron beam orbit, either through that ID or through another ID elsewhere on the ring. In order to allow the users the freedom to change their ID gaps, the IDs must be very well tuned magnetically so that they do not perturb the stored beam orbit and thereby affect the stability of any user's x-ray beam. The specifications for the IDs called for a very high quality magnetic field, and the insertion-device vendor more than met these requirements. However, the requirements were determined based on the assumption that there would be an active local feedback system to partly compensate for the remaining field errors. Further refining of the tuning of the IDs has been carried out in order to reduce or even eliminate the need for the active local feedback.

Another goal of tuning the magnetic field of an undulator is to improve the quality of the spectrum of emitted photons. Again, the undulator vendor more than met the demanding requirements, but the phase error has been further reduced so as to improve the spectral performance over a wider range of energies. The phase error does not cause a large decrease in the first harmonic intensity, but the amount by which it decreases the

intensity in a given harmonic increases with the harmonic number. In fact, it goes as e^{-np^2} , where n is the number of the odd harmonic and p is the phase error in radians (Walker, 1993). Therefore, the effect of a 5° phase error on the 5th and 7th harmonics would be to reduce the intensity to 83% and 69% of the ideal intensity, respectively.

An essential component of the ability to tune IDs is the ability to make accurate measurements of their magnetic field. The ID Magnetic Measurement Facility (Burkel et al., 1993; Frachon et al., 1995) now is equipped with two magnetic measurement benches, one with 3 m of travel and the other with 6 m of travel. There is also a laboratory electromagnet and a prototype APS dipole magnet for calibrating coils and Hall probes. A variety of probes can be mounted on either bench so they can map out the magnetic field in the gap of an ID. These probes include a number of coils of various lengths and orientations and Hall probes. A recent addition to the probes is an axial Hall probe that is used to measure the transverse horizontal component of the magnetic field. Long, stretched-wire-type rotating coils are also mounted to each bench so that integrals of the field through an ID can be measured more directly than with point-by-point measurements. The reproducibility that is routinely attained for the first field integral measurements is better than 0.5 G-cm. Using a Hall probe, the first field integral reproducibility is better than 5 G-cm. That the reproducibility of the measurements also applies in the long term has been shown by Hall-probe measurements of an ID that repeated with an rms difference of 2 G-cm after a period of one year.

In order to refine the magnetic field, tuning techniques have been developed. After the alignment of the magnetic structures has been checked and adjusted as necessary, the primary means of tuning the magnetic field is

shimming. Different sizes, shapes, and placements of small shims are used to adjust different aspects of the magnetic field. For most of the tuning techniques, the shims are placed on top of the magnets rather than on the poles because the magnetic structure was designed with the magnets recessed by a small amount compared to the poles. This allows shims to be placed on the magnets without affecting the achievable minimum gap. Shims can be placed along the ID as needed to straighten the trajectory and to decrease the phase error, thus helping to ensure a high quality undulator spectrum (Vasserman, 1996).

One way in which an ID can affect the stored beam is if the first or second integral of the horizontal or vertical component of the field through the ID is substantial. Therefore, an important goal in the tuning of an ID is to minimize these integrals, and to minimize the change in the integrals as the gap of the ID is changed. None of the standard planar IDs have any active correction of the field integrals, so the users rely on this tuning for a stable beam in the ring despite someone else's ID gap being changed. A non-zero first integral means that the trajectory of a particle after it has passed through the ID is at an angle with respect to its incident trajectory. A non-zero second integral means that the trajectory is offset after passing through the ID. The second integral is also a measure of the average trajectory angle inside the ID, so that if it varies with gap then the angle of the emitted photon beam will also vary, and the user will see the beam move as the gap is changed.

Once the trajectory through the ID is reasonably straight, first and second integral tuning is accomplished mainly by changing the configuration at the ends of the ID. A number of aspects of the end configuration are used in the tuning, including adjusting the

strength of the end magnets, changing the height or shape of the last two poles (in ways that do not affect the vacuum chamber clearance at minimum gap!), or adding shim material to the gap faces of the magnets or between two magnets on the side of a pole. Each of these changes has its own effect on the magnetic field integrals, and its own gap dependence to the effect. With some of the changes, the size of the effect varies even between nominally identical IDs, so it may be difficult to know a priori what will work best.

The IDs are also tuned to minimize their integrated multipole moments. If the integral of the field through the ID possesses a substantial quadrupole, sextupole, or octupole moment, that could affect the focusing and/or coupling of the particle beam.

4.1.2 Field Quality Achieved

Tuning techniques have been applied to fine-tune the magnetic fields of all the IDs. As more experience has been gained in tuning, the field quality achieved has improved. Over the past several shutdowns, installed IDs have been removed from the storage ring in order to install an improved design for the maximum gap hard stop. While the devices have been out of the ring, further refinement of the field quality has been carried out. This effort will continue as techniques improve. Fig. 4.1 shows the total variation of the vertical and horizontal first and second integrals of the field over the entire gap range, for the various IDs as they are now. Fig. 4.2 shows the phase errors for all of the undulators at a magnetic gap of 11.5 mm. The integrated multipoles through the IDs are also of importance due to the effect they have on the focusing and coupling in the stored particle beam. Fig. 4.3 shows the size of the variation in the normal and skew integrated quadrupole, sextupole, and octupole moments for the IDs.

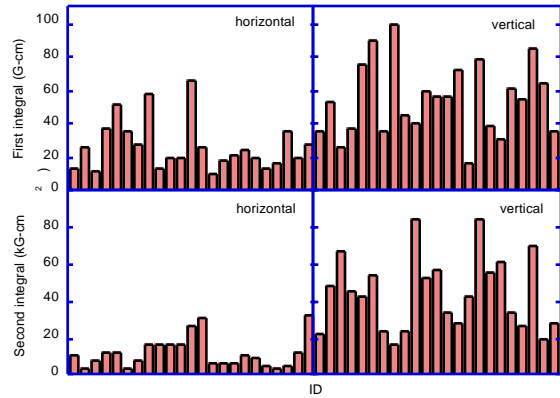


Fig. 4.1 The first and second integrals of the vertical and horizontal components of the magnetic field through the IDs are measured and tuned over the full gap range. The maximum and minimum values reached by each integral are determined. This figure shows the difference between those maximum and minimum values, for each ID.

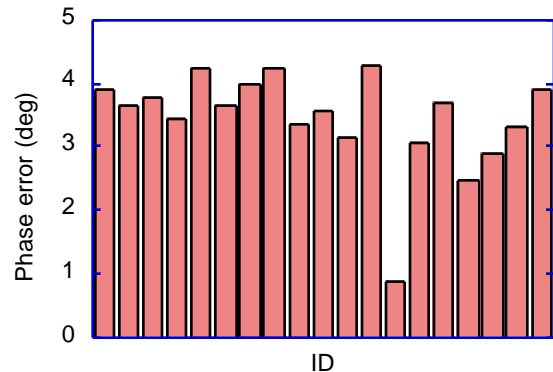


Fig. 4.2 The phase error at a gap of 11.5 mm, as measured for all of the APS undulators.

4.1.3 ID Control Development

Insertion-device control system development is focused on extending control access to users, improving ease of use, expanding the control system to accommodate new types

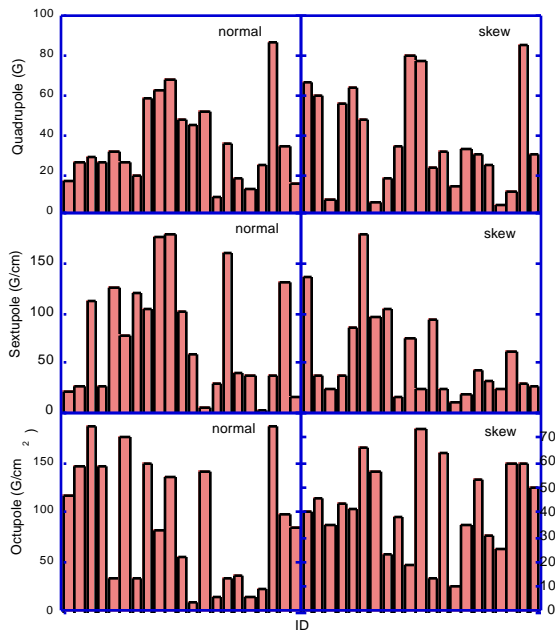


Fig. 4.3 The integrated multipole moments of the magnetic field through the IDs are measured and tuned over the full gap range. Maximum and minimum values for each moment are determined. This figure shows the difference between those maximum and minimum values, for each ID.

of IDs and improving system reliability. Eighteen undulators have been installed in the storage ring: 16 undulators A, 1 wiggler A, and 1 elliptical multipole wiggler.

The control of the IDs installed into the storage ring is integrated into the APS EPICS computer network with a dedicated IOC for each straight section. Controlled parameters include upstream and downstream drive motors that allow parallel or tapered positioning of the magnetic structure, linear absolute encoders for position monitoring, absolute rotary encoders for redundancy, and protective limit switches and interlock circuitry. Operators and users can monitor status and initiate actions from the control room or from computers located in offices or on beamlines. Security is maintained by the

use of a process variable server that allocates control according to predefined access tables.

The control system has been designed to enable users to control the ID on their own beamline simply and easily without involving facility operators. To this end, the control system has been developed to be friendly and easy to use but to be rugged and completely self protecting. Users can select a parallel gap position, a tapered gap position, or a desired first harmonic energy. The IDs have been designed and carefully tuned to eliminate any coupling between beamlines. Tests have shown that ID gap changes can be made in any or all sectors simultaneously without impacting the other users. All possible failure modes are continuously monitored, and users are prevented from inadvertently moving the ID in a manner that could damage the ID or the storage-ring vacuum system. The IDs are protected against motor stalls, encoder failure, excessive taper, and exceeding minimum and maximum limits. A software limit for commissioning can be set by the Floor Coordinator to administratively protect against excessive x-ray power during the commissioning of a beamline. If a problem should arise, the system will latch in its current state and a message will alert a user to the need to notify a Floor Coordinator to obtain expert assistance. An automatic log records the status changes and any errors that occur.

The interface to the ID control is implemented with the channel access features of EPICS. Control screens have been provided for users operating UNIX systems with EPICS (Fig. 4.4), or alternatively, users are able to design their own screens using variable names and descriptions that are readily available through the XFD Operations home page on the World Wide Web. CATs are asked to

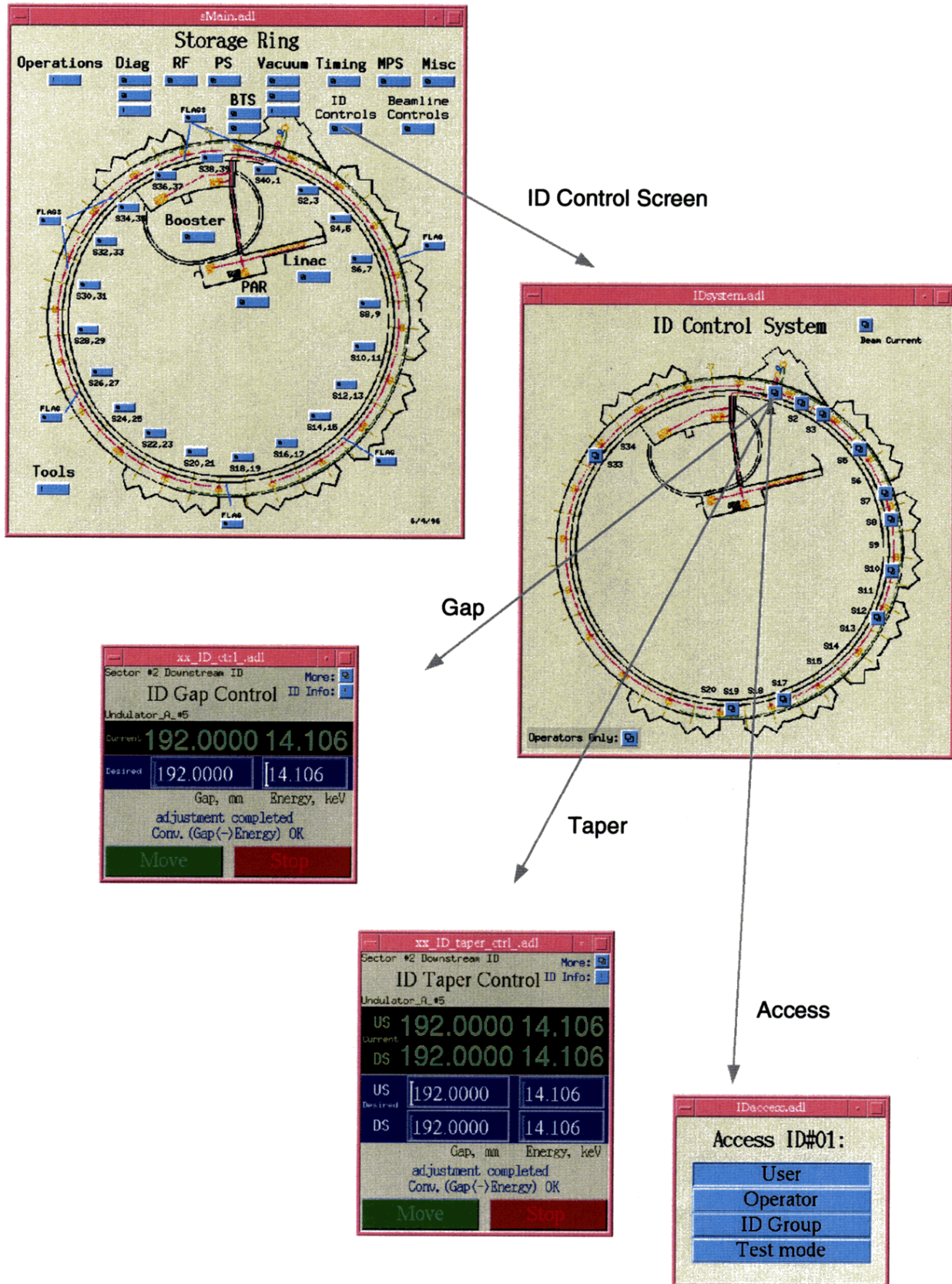


Fig. 4.4 EPICS screens available to users for control of undulator A and wiggler A.

provide a list of computer names and user names that are to be given access for control of the ID for their beamline. Only these authorized persons, Floor Coordinators, and system maintenance personnel are able to change gap positions.

The elliptical multipole wiggler (EMW) is a unique ID that has been installed in Sector 11 of the storage ring for polarized x-ray studies. In addition to the hybrid permanent magnet structure, it contains a horizontal field electromagnet that can alternate polarity at up to 10 Hz. The EMW control system consists of the standard controls for the vertical gap along with controls for the 1000 amp electromagnet supply and correcting coil supplies. The correcting coils are energized through an arbitrary function generator that allows the field to be varied so as to reduce the field integral of the electromagnet at positive and negative polarity and during the transitions. EPICS control screens have been generated to allow the EMW operator to vary all of the parameters during commissioning, but further work is required to reduce the controls to the relevant set for casual users and to simplify execution.

4.1.4 ID Vacuum-Chamber Development

A number of considerations in the design of undulators drive the design of the vacuum chamber to small gaps. On the other hand, particle beam transport considerations require the largest possible aperture. The competing requirements demand a vacuum chamber design with minimum chamber wall thickness, close tolerances for straightness and flatness to enable precision alignment, as well as mechanical and thermal stability. In addition, a

low outgassing rate, achievable manufacturability, low maintenance, and high reliability are also desirable.

During the last five years, a new approach to the design and fabrication of extruded aluminum vacuum chambers for IDs was developed at the APS (Trakhtenberg et al., 1996). Versions of the vacuum chamber, with vertical apertures of 12 mm and 8 mm, and lengths of 2.5 meters and 5 meters were manufactured and tested. Twenty chambers were installed in the storage ring and successfully integrated into the APS vacuum system. All have operated with beam, and 16 have been coupled with IDs.

All of these vacuum chambers have a wall thickness of 1.0 mm at the beam orbit position. Figure 4.5 shows a typical cross section. The chambers are fabricated by extruding 6063 aluminum alloy to form a tube with the desired internal shape (a) and machining the exterior to finish dimensions (b) and (c). The design utilizes a rigid strongback that limits deflection of the chamber under vacuum despite the thin wall.

In order to achieve and control the required vacuum, the ID vacuum chamber is equipped with a set of vacuum pumps and vacuum gauges. The total pumping capacity is achieved by combining two ~5-meter-long nonevaporable getter (NEG) strips with an average pumping speed of ~6 l/(sec cm), a 30 l/sec ion pump, and a 220 l/sec lumped NEG pump in each end box.

In addition to the pumps, the end boxes also accommodate transition sections, an x-ray absorber, and vacuum analyzers. The transition section in the upstream box is a water-cooled copper block that provides a smooth

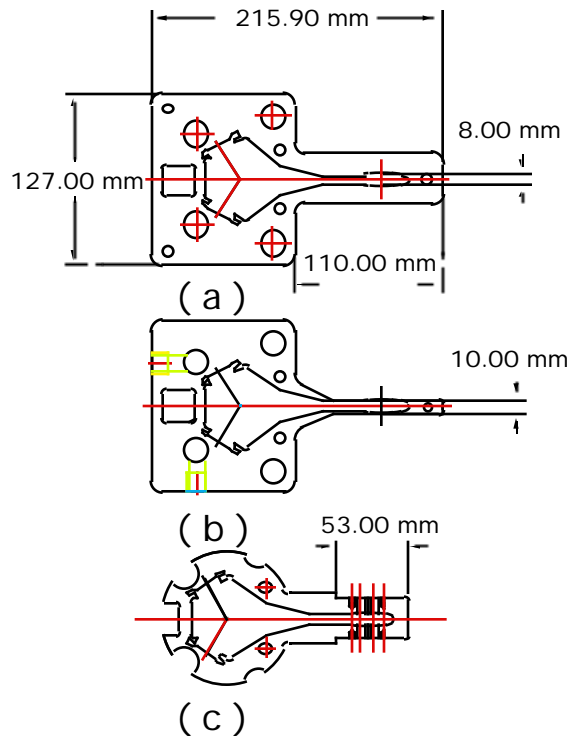


Fig. 4.5 Cross section of the 8 mm ID chamber. (a) extrusion, (b) after machining, (c) end geometry showing the locations of beam position monitors.

transition between the aperture of the ID and storage-ring vacuum chambers. The transition block in the downstream box is not water cooled. Both transition sections must be installed to avoid impedance mismatches that would affect the positron beam. The x-ray absorber is located in the downstream end box. It prevents the bending-magnet synchrotron radiation from penetrating the vacuum valve. Thermal calculations show, and experiments with installed chambers verify, that under relatively moderate cooling conditions, the temperature rise on the surface of the transition block or on the x-ray absorber does not exceed 110°C with a 300 mA positron current in the storage ring and under

maximum x-ray beam missteering. Figure 4.6 shows the layout of the ID vacuum chamber.

During the last year, 14 aluminum ID vacuum chambers were installed in the storage ring. Each chamber was certified at a pressure below 2×10^{-10} Torr prior to installation, and vacuum performance of the chambers was monitored with and without beam present. Initial installed pressure without beam is typically $1\text{-}5 \times 10^{-10}$ Torr (Fig. 4.7). Photo-desorption from synchrotron radiation raises the pressure during beam operations to about 2×10^{-9} . After several weeks of beam conditioning, pressures during beam operation decline to $< 1 \times 10^{-9}$ (Fig. 4.8).

Alignment of the vacuum chamber on its support is routinely accomplished using optical techniques to a precision of $\pm 75\ \mu\text{m}$ over the entire surface. This allows minimum insertion-device pole gaps to be obtained. All of the installed undulators can achieve a minimum gap of 10.5 mm while maintaining clearance from the chamber. At the present time, the minimum gap of all chambers is administratively set to 11.0 mm. As more experience is gained with the ID controls and the mechanical structure of the gap separation mechanism, the minimum allowed gap will be decreased to the mature phase value of 10.5 mm.

Experience elsewhere with stainless steel chambers and ST707 NEG material suggested the possibility of levitating dust particles of ferromagnetic material into the beam aperture of the ID vacuum chamber during ID operations. The signature would be a sudden drop in the lifetime of stored beam due to collisions with the levitated particle. No evidence of this effect has been observed at the APS.

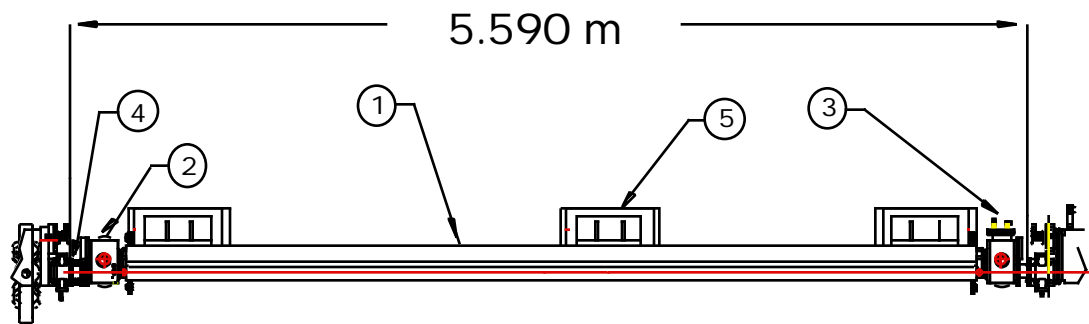


Fig. 4.6 Layout of the 5 m ID vacuum chamber. (1) ID chamber, (2) (3) stainless steel end box, (4) bellows, (5) support structure.

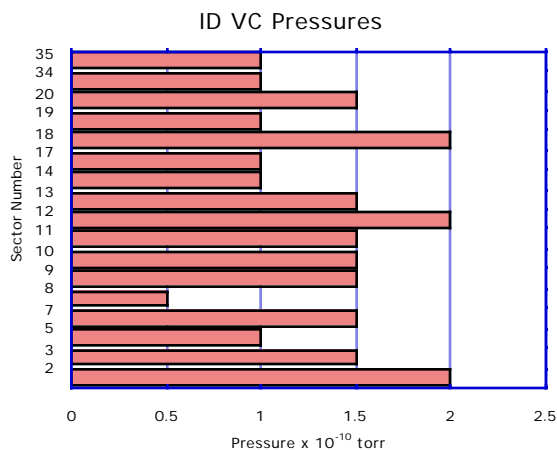


Fig. 4.7 Typical pressures for ID vacuum chambers installed in the storage ring.

4.1.5 5-mm-Aperture ID Vacuum Chamber

The standard 8-mm-aperture chamber with 1 mm wall thickness allows a minimum gap of 10.5 mm after allowing 0.250 mm on either side of the chamber for variations in straightness, flatness, and ID pole height variations. Because the gap separation mechanism of undulator A is designed to be able to withstand the magnetic forces at a minimum gap of 8.5 mm, it is desirable to have a vacuum chamber that takes full advantage of the

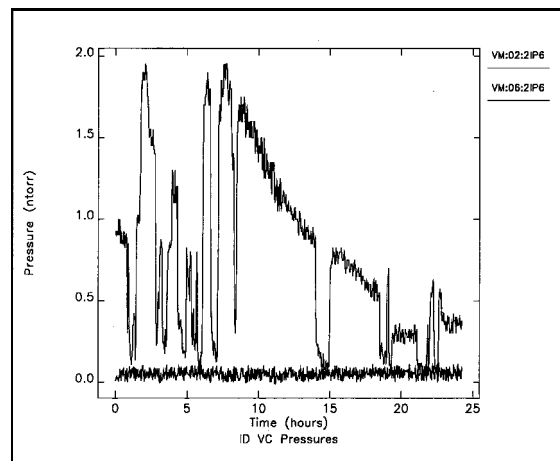


Fig. 4.8 Effect of beam-induced photo-desorption on an ID vacuum chamber. The upper trace is for a newly installed chamber in Sector 6. The lower trace is for a previously installed and well-conditioned chamber in Sector 2. The maximum stored current was 80 mA.

capabilities of the ID. A 5-mm-aperture extrusion was designed and fabricated and successfully machined to the same exacting tolerances as the standard 8-mm-aperture chamber. The chamber end geometry was tapered to 12 mm aperture to enable use of the standard end box. The chamber was welded, assembled, certified for vacuum, and

completely prepared for installation into the storage ring. Current plans call for a test installation in the storage ring in an unoccupied sector sometime during late 1997 or early 1998. A decrease in the size of the NEG pumping channel in this chamber relative to the standard 8 mm chamber results in somewhat worse vacuum conductance. During the test, the positron beam behavior will be monitored closely to detect any adverse effect on the beam lifetime or emittance. After the tests, the chamber will be removed from the storage ring for reinstallation in a sector where the full capabilities of the undulator A are needed.

4.1.6 EMW Vacuum Chamber Development

As described previously, the EMW utilizes both a vertically oriented permanent magnetic field and a horizontally oriented electromagnetic field. The design incorporates a 3100-mm-long stainless-steel vacuum chamber of rectangular cross section, with outer

dimensions of 69 mm wide by 22 mm high outer and a wall thickness of 1.2 mm (Den Hartog et al., 1996). Figure 4.9 shows the 5 m straight-section vacuum chamber assembly for the EMW. The magnet structures completely surround the chamber on all four sides, positioned only 1 mm from the chamber when in use. This precludes use of an "antechamber," as used in the standard insertion-device vacuum chamber. The standard chamber uses electrically activated NEG strips running the length of the chamber on the antechamber side for UHV pumping.

Given the constraints of the magnet geometry and the chamber length, two approaches were pursued for effective UHV performance. Both approaches utilize lumped NEG and ion pumping at either end of the chamber. One approach uses no additional pumping over the length of the chamber, relying on thorough cleaning and baking to minimize surface outgassing. The other method uses strips of sintered NEG material in diagonally opposed corners of the chamber top and bottom. The NEG material would be activated by heating

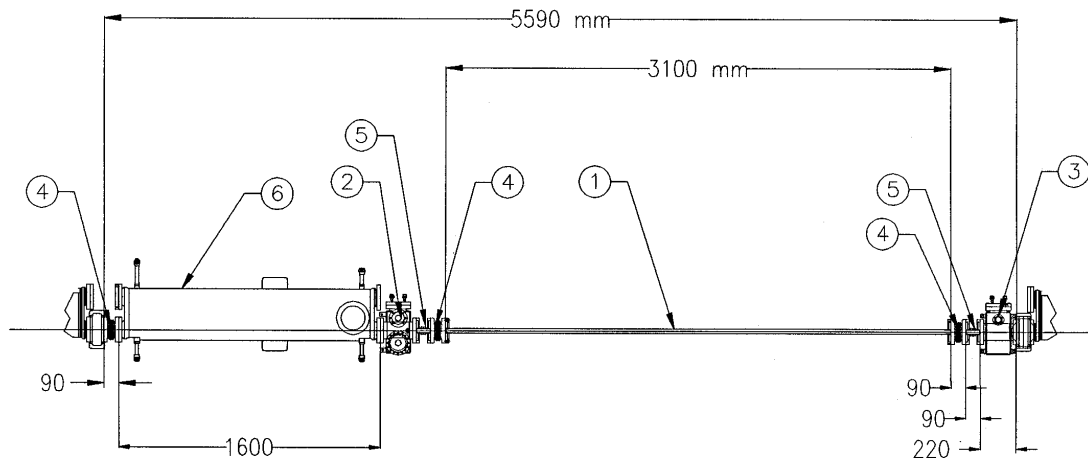


Fig. 4.9 General layout of the APS EMW vacuum chamber: (1) EMW vacuum chamber, (2) upstream end box with transition section, (3) downstream end box with transition section, (4) bellows, (5) BPM insert, (6) short storage-ring vacuum chamber.

the chamber. Both approaches are complicated by the need to entirely assemble the EMW magnet structures prior to closure of the vacuum system. The system used for *in situ* heating in either approach must maintain the permanent magnet structures below 35° C. Activation of the NEG strips requires heating the NEG material to at least 250° C.

As shown in Figure 4.10, the heating system uses copper plates in contact with the outside of the vacuum chamber. A total of four plates is used, covering most of the chamber length on the top and bottom. A 1 kW heater is mounted to each copper plate. Contact between the heaters and plates, and between

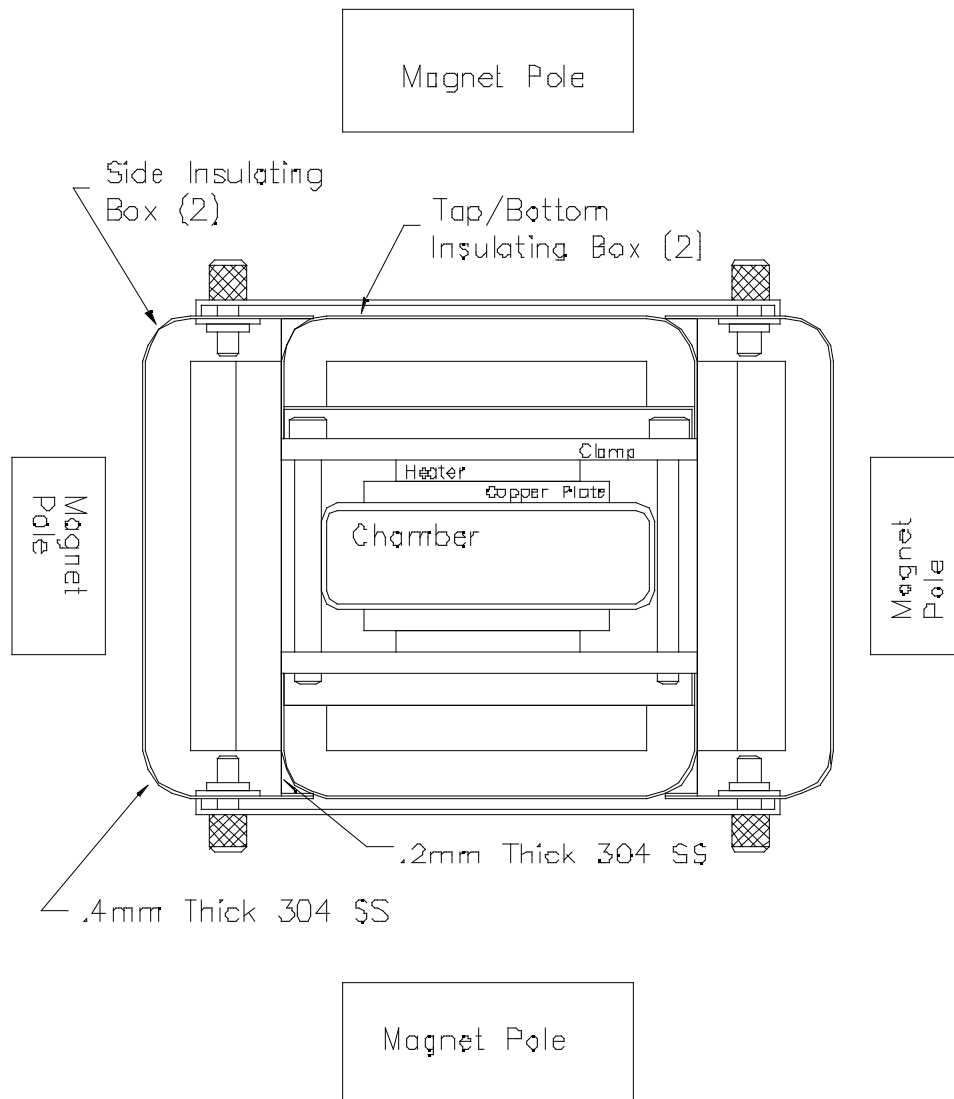


Fig. 4.10 Detail of *in situ* bakeout heaters for EMW vacuum chamber.

the plates and the chamber, is maintained with clamps held together with screws. Insulating boxes encapsulate the heating assembly. These boxes are made of thin stainless steel and are filled with layers of ceramic fiber insulation. The insulating boxes are held in place with thin stainless-steel channels, fixed to the side boxes with knurled screws. The entire heating and insulating system can be installed within the EMW structure after the magnet assemblies have been retracted.

While an acceptable pressure for installation had been achieved with the NEG-pumped chamber, it was not clear that the heat-activated NEG material provided a clear benefit. Heating the NEG material from the outside meant that the activated NEGs were subjected to heavy outgassing from the hot chamber, reducing their pumping speed and capacity upon cooling. Thus, the third test focused on the chamber without NEG pumping. The cleaned chamber was assembled, the copper strips were thoroughly cleaned to remove the sulfide/oxide scale, and the heating/insulating system was reassembled. The chamber was heated to 150°C. The heaters were at 225°C and the outside of the insulating box reached a maximum of 61°C. With ion pumping and activation of the other NEGs, a pressure of 1.7×10^{-10} Torr was obtained, better than the level of the NEG-pumped chamber. This chamber was used for the EMW installation.

4.1.7 Development of a Novel Vacuum Sealing Technique

A common feature of the ID vacuum chambers is the use of bonded aluminum and stainless steel in bimetallic transitions, which allow the joining of stainless-steel and aluminum parts. A roll-bond joint formed with a layer of 304 stainless-steel alloy, a layer of pure aluminum,

and a layer of 2219 aluminum alloy, provides a transition from the main chamber body (of 6063 aluminum) to the stainless-steel conflat flanges.

In the process of vacuum testing these chambers, several small vacuum leaks were discovered in the bonds of a few of the chambers. Twenty-six UHV vacuum chambers were fabricated using these transitions, twenty-one for use at the APS, four for the BESSY II project, and one for the ESRF. In these chambers, this sandwich plate was utilized for 52 standard end joints and for 24 circular ports for the BESSY II collaboration. Of the 52 standard end joints, leaks have been detected in five joints. Of the 24 BESSY II ports, leaks were detected in six joints.

To repair these leaks and prepare the chambers for use in an ultrahigh vacuum, high radiation dose environment, a completely new method was tested using high velocity oxygen fuel (HVOF) metal powder spray deposition. An HVOF system accelerates a powder of the selected coating material to supersonic velocities by injecting the powder into a combustion chamber and out through a nozzle with the combustion products. A variety of coating materials can be used including many metals and alloys, as well as ceramics. The high momentum of the particles creates a deposit with high adhesion, fine grain, and low porosity. It is these features that suggested its use for sealing small vacuum leaks. The desired seal must introduce no contaminants into the system, particularly hydrocarbons, must be capable of withstanding repeated bakeouts at 150°C, and must be immune to radiation damage from x-rays and bremsstrahlung.

To test the feasibility of the process, samples were prepared and sent to vendors to test different coating processes and materials. One

of the samples was sealed completely by using the HVOF process and a Cr₃C/NiCr coating, verifying the potential of the process.

The HVOF process is subject to a great number of variables including surface preparation, powder mixture, particle mesh, feed rates, gas mixture and consumption rates, spray distance and deposition rate, coating thickness, number of coatings, substrate temperature, and environmental conditions, such as humidity. Each of the ID vacuum chambers was sprayed under different conditions, making generalized conclusions difficult if not impossible without increasing the number of samples. Results vary from sealing the leak, to no change, to actually increasing the size of the leak (probably due to thermal effects). Given the proper set of conditions, however, it has been shown that it is possible to seal vacuum leaks in a manner that is completely consistent with ultrahigh vacuum requirements. Further tests are planned to define the proper parameters.

4.1.8 ID Installation and Commissioning

The first ID was installed in the storage ring in August 1995, after the installation of the first ID vacuum chamber. This first chamber had an aperture of 12 mm. The very satisfactory initial tests that were run at the time found that the effect of moving the undulator gap on the stored particle beam was smaller than the requirements—in fact, it was only measurable above the noise after statistics had been gathered for many minutes! Harmonics could be seen clearly in the undulator spectrum to over 100 keV. The x-ray beam size and angular divergence were also used to determine the emittance of the stored particle beam. These results were reported at the 1995 Synchrotron Radiation Instrumentation

Conference (Cai et al., 1996a, 1996b). The undulator was subsequently removed from the storage ring to allow commissioning of the ring to proceed with the installation of the smaller (8 mm) aperture ID vacuum chambers.

In the fall of 1995, installations of IDs on the 8-mm-aperture vacuum chambers began. In January 1996, there were three IDs installed. At the end of March 1997, there are a total of 18 IDs installed around the ring (Table 4.1).

Note that there are two undulators installed in Sector 2. The straight sections are long

Table 4.1 IDs Installed on the Storage Ring as of March 1997

| Sector | ID installed | Period length (mm) |
|--------|--------------------|--------------------|
| 1 | undulator | 33 |
| 2 | undulator | 33 |
| 2 | undulator | 55 |
| 3 | undulator | 27 |
| 5 | undulator | 33 |
| 7 | undulator | 33 |
| 8 | undulator | 33 |
| 10 | undulator | 33 |
| 11 | elliptical wiggler | 160 |
| 12 | undulator | 33 |
| 13 | undulator | 33 |
| 14 | wiggler | 85 |
| 17 | undulator | 33 |
| 18 | undulator | 33 |
| 19 | undulator | 33 |
| 20 | undulator | 33 |
| 33 | undulator | 33 |
| 35 | undulator | 18 |

enough to accommodate two of the standard-length (2.4 meter) IDs. Other sectors may install a second ID in the future if, for example, a different period-length undulator would significantly increase their brilliance in some particular wavelength range. The users close the gap of whichever undulator they want to use at that particular time. Some of the undulators are longer, however, and occupy the entire straight section, such as the elliptical wiggler and the 18-mm-period undulator that is being used by the APS Diagnostics Group to monitor beam quality.

Initially, the gap of an ID was moved only by an ID Group member, only from the Main Control Room, and only with the full knowledge of the accelerator physicist who was operating the storage ring. After the initial testing of the effect of an ID on the stored particle beam showed that the effect was barely measurable, however, permission was routinely given to change the gap as requested by the user, without the need to inform the ring operator. Control of the IDs was then entrusted to the Floor Coordinators, who could move the gaps from computer terminals in their offices on the experimental floor as requested by the users. More recently, users are being given the freedom to control the gap of their ID themselves. As of the run time in March 1997, users in ten sectors now may change their ID gap whenever and however they wish during normal user beam time. For now, Floor Coordinators still open all ID gaps before beam injection, then return the gaps to their previous values once injection is complete.

4.1.9 Storage Ring Measurements

Careful measurements of the magnetic field of an ID are made to predict the effect of the ID's magnetic field on the stored particle beam.

The measurements are used to tune the magnetic field, as described above, to minimize undesired effects on the stored beam. The real test of what has been achieved, however, is to install the ID in the storage ring and to measure the actual effect it has on the stored beam. The gap of the ID is cycled between minimum gap and, typically, 45 mm. The global beam position feedback in the storage ring is turned off for these experiments. The variation in the beam position monitor (BPM) readings between the two different gaps is recorded for BPMs all around the ring. Calculations of the closed orbit are then performed in which a kick is added at the position of each end of the particular ID being tested, and the size of the kicks adjusted to fit the observed closed orbit change. These kicks are then used to compute the first and second field integrals. The integrals determined in this way agree with the first and second integrals of the magnetic field through the ID as measured in the APS Magnetic Measurement Facility.

Another important measurement of the effect of an ID on the stored beam has also been carried out. The gap on one ID was moved through its full range of travel while the position of the x-ray beam was observed in a different sector. No movement of the x-ray beam in the second sector was seen, to a sensitivity of 4 microradians. Work is in progress to repeat this measurement with an even higher sensitivity. Note that this is with no active local feedback correction on the particle beam orbit; only global feedback was in operation.

The motion of the x-ray beam due to changes of the gap in the ID producing the beam has also been measured, using a zone plate to image the beam onto a position-sensitive detector. The position of the x-ray beam was found to be constant to within the

3 microradian sensitivity of that measurement, again with no local active feedback on the particle beam.

4.1.10 Spectral Performance

The APS undulator A provides high brilliance x-ray radiation in the 3.2-45 keV spectral energy range. In order to characterize the performance of the undulator, absolute measurements of the undulator brightness as a function of angle and energy have been made. The quality of the undulator magnetic field may be verified by observing the high order harmonics of the undulator radiation. Undulator brightness depends on the particle beam divergence and energy spread.

These measurements may have to be made under conditions of high incident beam power and high incident beam power density. The experimental setup is schematically shown in Fig. 4.11. Upstream of the two spectrometers, a water-cooled conical pinhole with an exit diameter of 0.8 mm was used to remove a substantial fraction of the undulator power from the beam. Vertical and horizontal water-cooled slits define the angular acceptance of

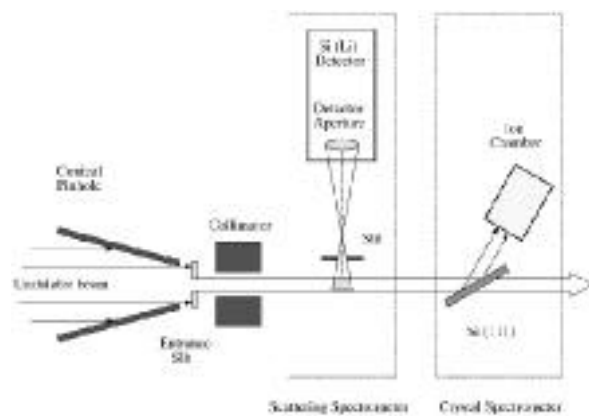


Fig. 4.11 The experimental setup used to measure the spectrum of x-rays from an undulator.

the incident beam. In order to collimate the bremsstrahlung radiation, a 100-mm-thick tungsten block with a 5-mm-diameter hole was placed downstream from the slits. The pinhole, slits, and the tungsten collimator were placed in a helium enclosure and were carefully shielded with lead. Two spectrometers were used for absolute flux measurements. The first uses the scattering from a gas whose differential cross section is well known, combined with an energy-dispersive detector. While the use of an energy-dispersive detector can provide convenient and fast absolute flux and linear polarization measurements, in order to obtain more accurate measurements of the odd undulator harmonics, it may be necessary to use a crystal spectrometer. The crystal spectrometer employs a Si (111) crystal and an ion chamber detector filled with nitrogen gas. The single-reflection geometry makes spectral measurements quite insensitive to thermal distortion of the crystal because the integrated reflectivity of the crystal can be calculated by dynamical diffraction theory even in the presence of a moderate thermal bump. The efficiency of the ion chamber was determined by calculating the fraction of x-rays absorbed in a 100 mm active path. The silicon crystal was characterized using surface topography and x-ray diffraction and was found to be a perfect crystal.

A comparison of experimental results versus calculations for on-axis flux tuning curves for the first, third, and fifth harmonics of radiation for undulator A is shown in Fig. 4.12. An aperture of $150 \times 75 \mu\text{m}$ was located 28.9 m from the source. The typical storage-ring current was 40 mA. There are two calculated curves for the third and fifth harmonics because of different coupling constants during the data collection (8.5% for small undulator gaps and 4.6% for large

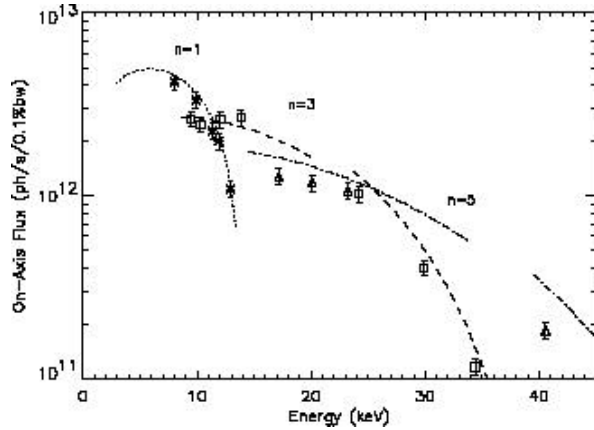


Fig. 4.12 On-axis flux of x-rays from an undulator as a function of energy. The first, third, and fifth harmonics are shown. The points are measured results; the lines are the results of calculations. There are two calculated curves for the third and fifth harmonics because the experimental measurements were made at two different times when the particle beam parameters were different.

gaps). Experimental results were normalized to a beam current of 100.0 mA. The error bars are $\pm 10\%$. The discrepancy between the measurements and the calculations can be attributed to (1) the magnetic field errors of the real device, which cause the intensity of the higher harmonics to be reduced from the ideal, and (2) the error in the emittance measurements, which are used for flux calculations. The anticipated reduction is most easily obtained by numerical simulations using the code UR for the practical case of including the beam emittance, the beam energy spread, and a finite size aperture.

The APS beam emittance was obtained by measuring the vertical and horizontal size and divergence of the undulator x-ray beam. Undulator radiation passes through a water-cooled conical pinhole, which reduces the incident power on the cryogenically cooled Si (111) crystal. This horizontally deflecting

Si crystal is vacuum sealed between two 150- μm -thick beryllium windows. A gold zone plate is used to form an image of the x-ray source. A platinum order sorting aperture was used to increase the contrast in the image. An energy-dispersive Si (Li) detector was located close to the image plane to measure the x-ray fluorescence generated from a sharp Ni knife-edge (K emission line) placed in the imaging plane. The beam size was determined from fluorescence intensity profiles measured when the knife-edge was scanned across the beam. The resulting rms source sizes are $300 \pm 25 \mu\text{m}$ in the horizontal direction and $60 \pm 9 \mu\text{m}$ in the vertical. Beam divergence measurements were performed by scanning a slit across the undulator beam in the vertical and horizontal directions, at a monochromator energy that is on the low energy side of the undulator harmonic. This energy is chosen because it substantially reduces the intrinsic undulator divergence contribution. The beam divergence was obtained by fitting the measured beam profile with a calculated one. The fitting gives the result of $25 \pm 2.5 \mu\text{rad}$ for horizontal divergence and $5.3 \pm 0.5 \mu\text{rad}$ for vertical. The corresponding horizontal (x) and vertical (y) emittances (obtained at a current of 20 mA) are

$$x = 7.5 \pm 6.0 \times 10^{-9} \text{ mrad}$$

and

$$y = 3.2 \pm 6.0 \times 10^{-10} \text{ mrad}.$$

The coupling constant ϵ , which is the ratio of the vertical to the horizontal emittance, thus becomes $4.3 \pm 1.3\%$.

The measured on-axis spectral brilliance (solid line), using the crystal spectrometer, and calculated on-axis spectral brilliance (dotted

line) of the undulator radiation from a 7 GeV electron beam at a gap of 15.8 mm ($K=1.61$) are shown in Fig. 4.13. The calculation included the measured magnetic field of the undulator, the electron beam emittance, measured at the time of the brilliance measurements, ($\sigma_x=6.9$ nm-rad, $\sigma_y=0.2$ nm-rad), and the design value for the electron beam energy spread (0.1%). The error bars are $\pm 18\%$, which includes systematic errors for flux and emittance measurements. As is clearly seen from the figure, the measurements are in remarkably good agreement with the calculation. The quality of the undulator magnetic field was verified by observing the high order harmonics of the undulator radiation. More than thirty harmonics can clearly be seen in Fig. 4.14, where the measurements performed at an undulator gap of 11.1 mm are shown along with the results of calculations that used the measured magnetic field.

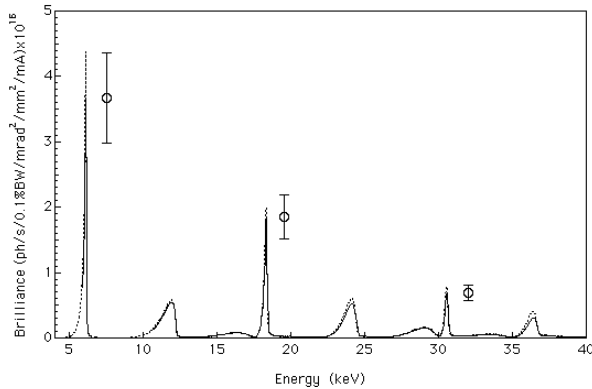


Fig. 4.13 The on-axis spectral brilliance is shown. The solid line was measured using the crystal spectrometer; the dotted line is from a calculation. The calculation included the measured field of the undulator, the measured electron beam emittance, and the design value for the energy spread.

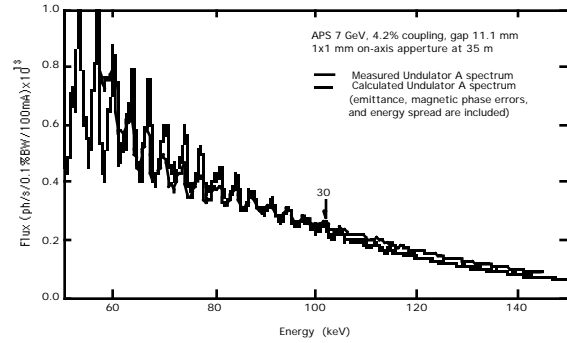


Fig. 4.14 The harmonic structure of the undulator radiation at higher energies. Harmonics as high as the 30th are clearly seen.

4.1.11 Computer Codes for Simulation of Synchrotron Radiation

Computer simulations of synchrotron radiation are invaluable for characterization of new IDs being installed in the storage ring. Generally, the simulation of the radiation can be divided into two categories—the first being simulation of radiation from an ideal device albeit with a real electron beam, the second being simulation of the real device with the real beam. The simulation of real devices with the real beam is computing intensive but manageable with today's high speed workstations and personal computers with results obtained in typically one day of computing time. Computer codes for both categories have been developed in collaborative efforts at the APS, and a few results of these codes will be presented here.

Quite often it is not enough to have access to a computer code that, in principle, will solve a particular need because the code is difficult to use—either because of poor documentation or because of the complicated nature of the code.

In this regard, the use of graphical user interfaces for entering data and for displaying results has become important. A suite of programs for modeling radiation characteristics of ideal devices (real electron beams) and the interaction with optical elements has been developed and assembled into a package called XOP (x-ray optics utilities) using a common graphical user interface. This interface largely simplifies the execution of the codes and may be run without any prior knowledge of how to run a particular program.

4.1.12 XOP: A Graphical User Interface for X-ray Optics Utilities

The XOP interface contains a suite of programs of general interest to the synchrotron radiation community (Dejus and Sanchez del Rio, 1996). They are easy to use, fast, and the results are visualized and analyzed using the provided plotting interface—all tasks are performed without leaving the interface. The programs have been naturally divided into two general categories (Fig. 4.15a)—computer codes for generation of synchrotron radiation properties of undulators, wigglers and bending magnets, and codes for computation of optical constants, photon cross sections, mirror reflectivities, filter transmissions, crystal diffraction profiles, and multilayer reflectivities.

The interface, which was written in the IDL (interactive data language) programming language, runs on workstations for most flavors of the UNIX operating system including Sun Solaris, HP-UNIX and Digital UNIX. It is also available for PCs running Windows-95 and Linux. Other operating systems will be available as demand changes.

The package is stand alone, no commercial license is needed, and is available free of charge to non-profit organizations.

Figures 4.15b and 4.15c show the pop-up menu (Xus) for the code US (undulator spectrum) with the accompanying input menu for entering data and for setting parameters and options. In this example, the calculation of the flux spectrum through an aperture was chosen (size of aperture was chosen to approximately cover the central cone of radiation). The results are visualized and analyzed using the built-in plot interface Xplot.

The calculated emitted x-ray spatial distribution at select energies (near harmonic energies) has been verified experimentally. The single electron radiation pattern shown in Fig. 4.16a was calculated using the Xus interface and broadened with the introduction of the beam emittance of the stored beam. The broadened profile was successfully matched with the measured profile near the third harmonic energy by fitting the size and divergence parameters of the beam. Fig. 4.16b shows the result of the best fit and the measured beam intensity profiles (vertical only). The code was further verified experimentally by measuring the tuning curves of the *absolute* spectral flux for the first three odd harmonics of radiation (see section 4.1.10 on spectral performance).

4.1.13 UR: Computer Code for Simulation of Real IDs with Real Beams

The computer code UR (undulator radiation) has proven instrumental when predicting the spectral performance of the APS insertion

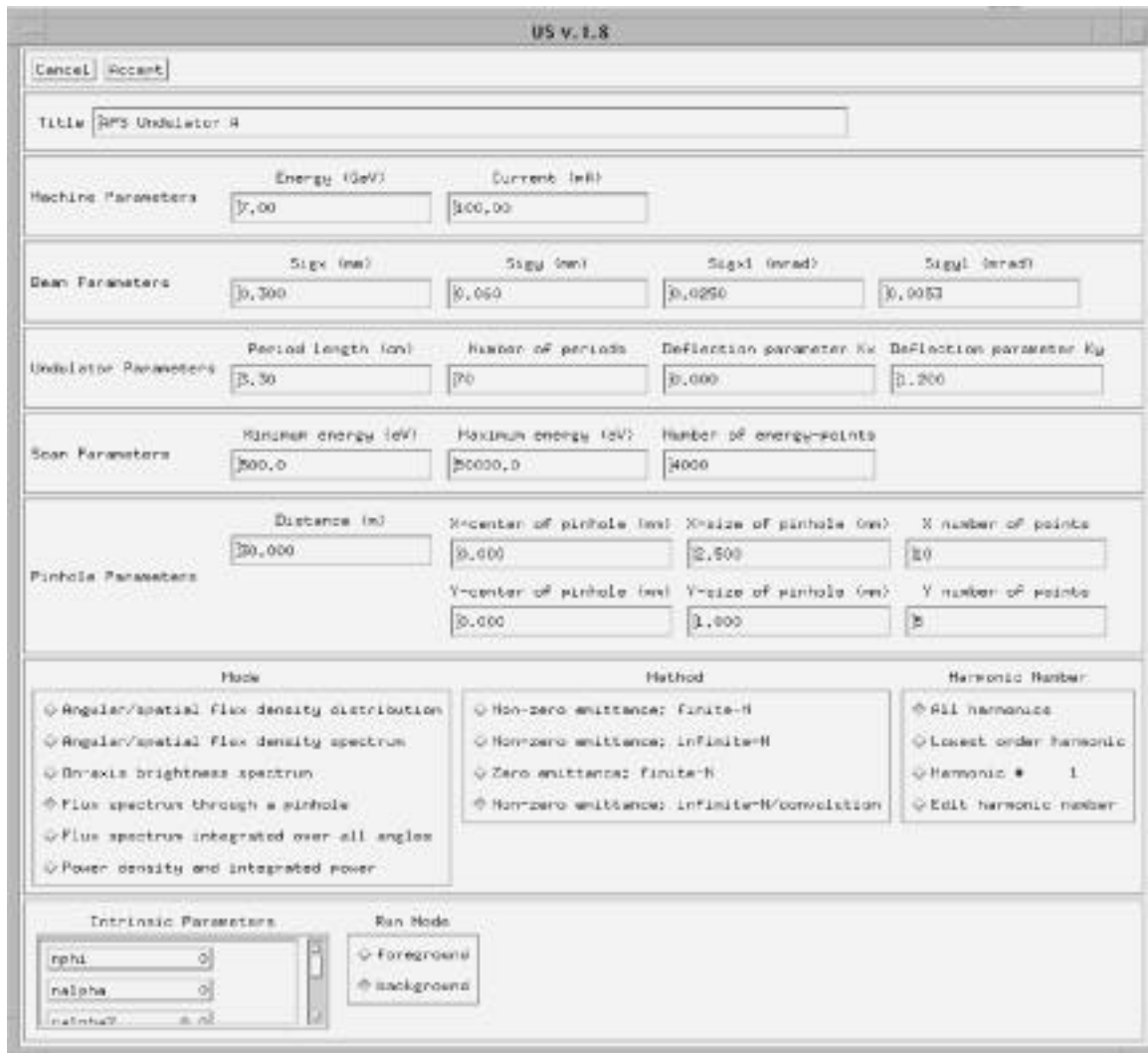
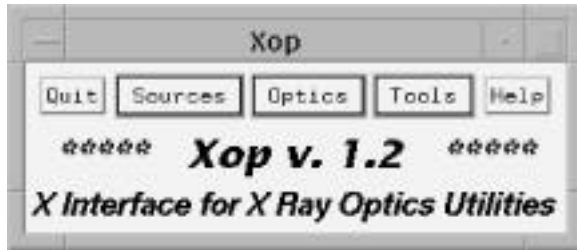


Fig. 4.15 (a) (upper left) The main menu of XOP with separate buttons for sources and optics utilities. (b) (upper right) Pop-up menu for the code US (Undulator Spectrum). (c) Input menu for the code US.

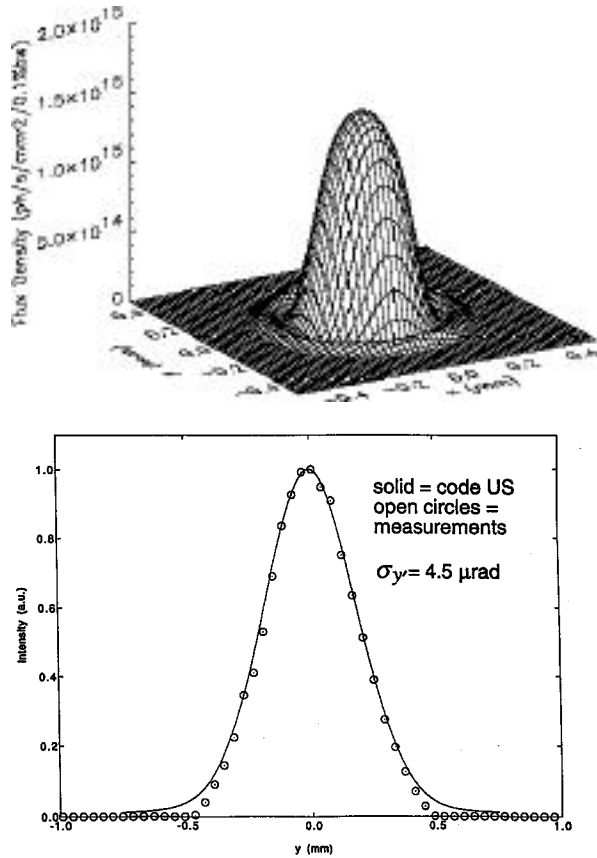


Fig. 4.16 (a) (top): Single electron radiation pattern at 32.8 m near the third harmonic energy (18.4 keV) for undulator A ($K=1.61$). (b) (bottom): Calculated and measured vertical beam intensity profiles of radiation at 18.4 keV for undulator A ($K=1.61$).

device on an absolute level. The computer code solves numerically the equations of motion (3-D) for an arbitrary magnetic field and calculates the radiation field at each time step as the particles are tracked through the device. The real beam emittance and beam energy spread and the actual magnetic field of the device are typically used in the calculations (Dejus and Luccio, 1994).

Experimental characterization of undulator A has been performed not only at low photon energies but also at high energies (> 50 keV) and comparisons of the measured and

calculated spectral flux have been made. The measured and calculated flux through an aperture (1×1 mm) located 35 m from the source for an undulator gap setting of 15.5 mm ($K = 1.63$) is shown in Fig. 4.17. The 11th harmonic is seen at 66 keV, and its shape and structure has been influenced largely by the non-perfect magnetic field in addition to the effect of the beam emittance and beam energy spread. All three effects make the high harmonics show a complicated pattern—it should be noted that the code is able to predict all harmonics (up to number 29 at 170 keV) including the detailed sub-structure of the harmonics.

4.1.14 Radiation Exposure of the IDs

NdFeB magnets are known to be sensitive to radiation damage, and some work has been done in the past, by others, to determine the radiation susceptibility of the NdFeB. Much of the work that has been done, however, is not directly applicable to ID magnets because the spectrum of radiation used in the study or its makeup (e.g., neutrons as opposed to electrons or photons) is not the same as will

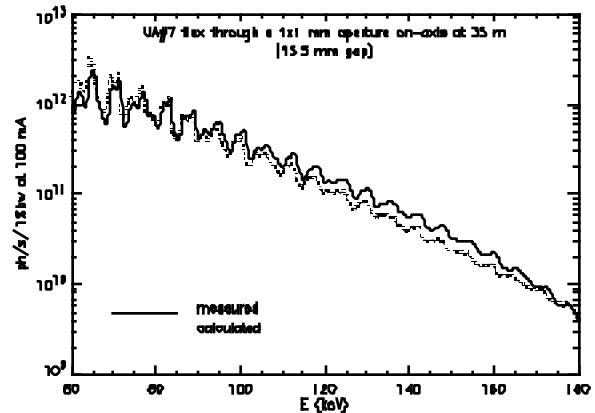


Fig. 4.17 Comparison of measured and calculated spectra for undulator A ($K=1.63$).

be present in a storage ring. Also, Nd magnet technology has developed rapidly in recent years so that the magnet material used in the APS IDs was not available eight years ago. The effect of stabilization of the magnets is unclear, and there may be variation in radiation sensitivity between magnets from different vendors as well (see Chavanne et al., 1996).

There is no doubt, however, that the radiation exposures received by ID magnets are sufficient to cause demagnetization. This has been shown at ESRF by an ID that showed partial demagnetization after being installed for a year (see Colomp and Brauer, 1993). The best estimate for the total dose received by that ID is 5.1 to 6.8 Mrad at the first magnet. At the upstream end of the device, about 7% of the peak field was lost due to demagnetization.

Not all the radiation to which an ID could be exposed will contribute towards demagnetization, however. Experiments have been reported (Okuda et al., 1994) in which magnets were irradiated with 17 MeV electron beams and 1.17 MeV ^{60}Co γ -rays. Whether the energy quanta are electrons or photons probably does not matter, but the energy of the quanta does make a difference. No demagnetization was seen after exposure to 280 Mrad of 1.17 MeV γ 's, but there was a 9% flux loss for the NdFeB exposed to 260 Mrad of 17 MeV electrons. The radiation-demagnetized magnets were subsequently remagnetized to essentially full strength.

Clearly, then, one needs to know the spectrum of radiation to which the magnets are exposed in order to predict the likelihood of damage.

An experiment was carried out at the APS to determine whether the dose rates being measured at the IDs using film dosimeters and thermoluminescent dosimeters (TLDs) were from high or low energy quanta. A multilayered sandwich of alternating Pb and film dosimeters was placed so the dosimeters were approximately 30 mm directly above the positron beam, as shown in Fig. 4.18. The dose as a function of depth of Pb was measured, and the results are shown in Fig. 4.19a. For comparison, the absorbed energy as a function of depth in Pb due to a 6.3 GeV cascade is shown in Fig. 4.19b (data from Bathow et al., 1967). The depth at which the peak dose occurs is a function of the energy of the incident quanta. The similarity between these curves suggests that 7 GeV quanta made up a large fraction of the incident radiation in the APS test. This radiation is high enough in energy to demagnetize the magnets.

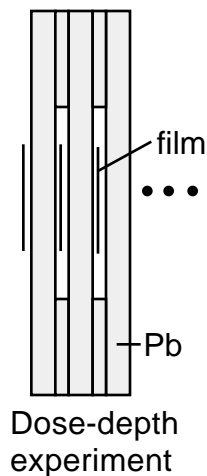


Fig. 4.18 Schematic of part of the experimental setup used for the dose-depth experiments. The setup consists of a 16-to-32 layer sandwich of film dosimeters between Pb plates.

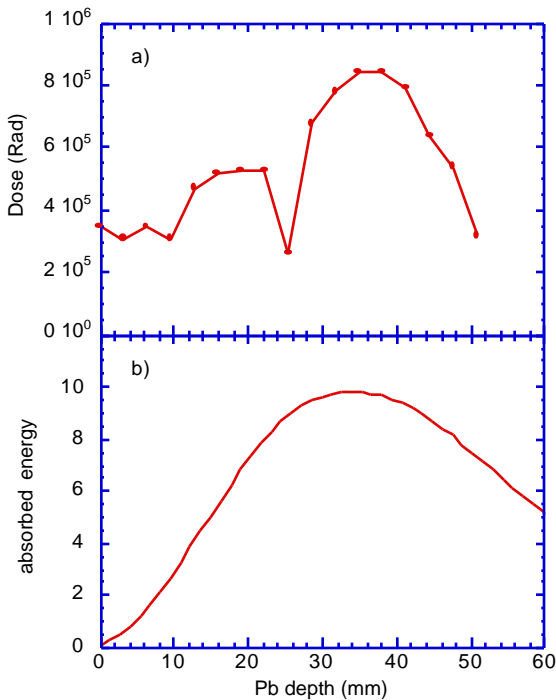


Fig. 4.19 (a) The results of the dose-depth experiment are shown. Each point is the reading from one film dosimeter. (b) For comparison, the published results (Bathow et al., 1967) of a simulation of the absorbed energy as a function of depth in Pb due to incident 6.3 GeV quanta were graphed.

The depth-dose experiment was repeated during the subsequent run. In that experiment, the peak dose occurred at a shallower depth, suggesting that some of the cascade had already taken place before the radiation reached the experiment. It may be that the spectrum of the dose reaching the ID varies strongly with events or beam characteristics that are specific to the particular run. More experiments will be conducted to further characterize the exposure.

Dose measurements made during the first running period with IDs installed and with the smaller gap vacuum chamber alerted us to the

need to provide some radiation shielding for the IDs. During much of that run, injection efficiency was quite low and for long periods of time beam was being injected even though it wasn't being successfully stored. When the dosimeters were removed and read out, two of the three installed IDs were found to have been exposed to extremely high doses. The response of the TLDs used flattens out at exposures over about 300 Krad, so it is difficult to know the actual dose to within a factor of 2, but it is estimated to have been as high as 5 Mrad on one ID and 1 Mrad on the other. The gap on the third ID had been kept open during the entire run, so its dose was only 52 Krad on the first pole. However, a second dosimeter that was placed to measure what the dose would have been for that ID if it had been at minimum gap for the entire run gave an estimated dose of 3 Mrad. The magnetic field of the undulators that have received the highest doses was rechecked, most recently in March 1997, and no demagnetization was found.

After these surprisingly high dose rates and knowing the experience at ESRF, it was decided that measures to reduce the exposures encountered by the installed IDs were warranted. As a result, IDs are now installed in the downstream part of the ID straight section whenever possible, and Pb shielding is installed in the open space upstream of the ID.

The Pb shielding that has been installed is more than 30 radiation lengths thick and should reduce the radiation levels to something too small to measure. The measured effect of the Pb gives us insights into the spatial distribution of the radiation. Fig. 4.20 shows the dose measured during a 3.5-week run by film dosimeters laid flat on the upper

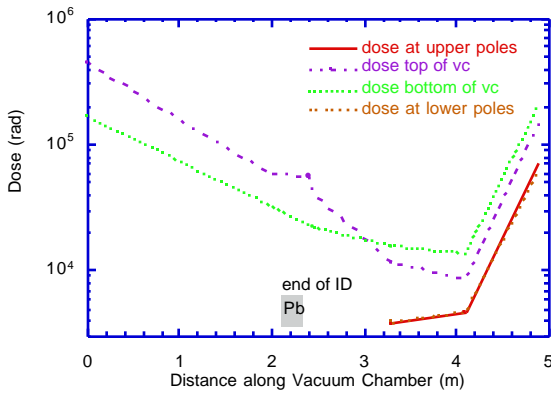


Fig 4.20 Doses measured using film dosimeters that were placed flat on the top or bottom of a 10-mm-outside-dimension ID vacuum chamber. Dosimeters were also placed on the faces of the pole of the ID, which was kept at 100 mm gap throughout the 3.5-week run. The position of the Pb shielding upstream of the ID is shown. The dose at the upstream end of the ID (marked on the graph) was too small to measure by this technique (<3000 Rad).

and lower faces of the (10-mm-outside-dimension) vacuum chamber and laid flat on the pole faces of the ID. This ID was kept at 100 mm gap throughout the run. The position of the Pb shielding is marked on the graph; note that it has no effect on the distribution of doses measured at the face of the vacuum chamber, despite the fact that there is no gap between the Pb shielding and the vacuum chamber. The Pb does dramatically reduce the dose at the upstream face of the first pole where the unshielded doses were highest; however, that point is not shown on the graph because the dose there was too small to measure. The Pb shielding has essentially no effect on the dose at the downstream end of the ID. This shows that while there is radiation traveling through the air above the vacuum chamber, there is also a non-negligible amount of radiation that

will reach the magnets of an ID at closed gap by traveling through the vacuum chamber. So although the shielding dramatically reduces the radiation dose at the upstream end of the ID, where it would otherwise be highest, it has essentially no effect on the lower dose levels at the downstream end.

Another means that is used to reduce the radiation dose to the magnets is to leave the ID gaps open when the IDs are not in use and, more specifically, to open the gaps for injection. Figure 4.21 shows the total dose measured during a 6-week running period at the first poles of each of the installed IDs. Dosimeters were also mounted immediately upstream of the first pole of each ID, at the same distance from the vacuum chamber as the dosimeter on the first pole would be if the

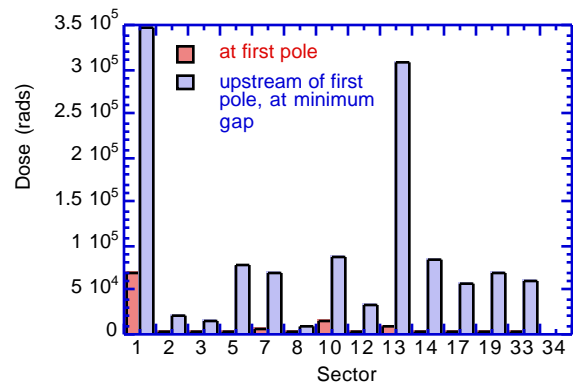


Fig. 4.21 Dosimeters were placed on the upstream face of the first pole of each of the IDs. There were also dosimeters placed on the vacuum chamber immediately upstream of the ID, at the same distance from the particle beam as the dosimeters on the poles would be if the ID were at minimum gap. Thus, the difference between the two bars in each sector shows the radiation exposure the ID was spared by not being at closed gap during the entire run.

ID were at minimum gap. Thus, the difference in dose rates indicates the amount of dose the ID was spared by having the gap open when the ID was not being used.

While these measures that have been taken to reduce the exposure of the IDs have been effective, they are not the final answer. One reason why is that not all IDs can be protected by Pb shielding because there isn't always enough space for the shielding. Another reason is that an eventual goal in the operation of the storage ring is to go to a "top-off" mode in which small amounts of beam would be injected frequently so that the beam current would be kept nearly constant. That way, the users would have a beam with constant brilliance. These frequent injections would need to be carried out with the ID gaps closed. In order to be confident that this would not be putting the IDs at risk, a better understanding of the origin of the dose is needed—it could be mainly coming from beam that is lost during injection, it could be a steady dose from the entire time the beam is operating, or it could be from particular beam-loss events. A means of monitoring radiation levels in real time to better understand the origin of the radiation is being sought. A better understanding of the causes of demagnetization and the dose at which demagnetization should be anticipated may allow us to run the storage ring in the way that best suits all the users, without risking damage to an ID and the resulting down time for the user of that ID.

4.1.15 Elliptical Multipole Wiggler

In addition to the standard planar IDs, there is also an elliptical wiggler installed in the ring now. This device was built jointly by the APS

and the Budker Institute of Nuclear Physics in Novosibirsk. It has planar arrays of magnets and poles to produce the vertical magnetic field component, just as the standard IDs do. The weaker horizontal field is produced by electromagnets. The device has a 16 cm period. The total number of poles is 36 for the electromagnets and 37 for the permanent magnet array. Thirty-two of the poles in each direction are full field. The user deemed it important to have an even number of full field permanent magnet poles so that the spatial distribution of radiation from the wiggler would be, in principle, symmetric above and below the beam axis. An even number of full-field electromagnet poles was expected to simplify the tuning of the field, because the demand for horizontal field quality is higher. The horizontal electromagnet field is designed to operate at a frequency of 10 Hz, at a peak current of 1 kA. This current produces a peak horizontal field of 997 G, or $K_x=1.5$. The peak vertical field is 9826 G at the minimum gap of 24 mm, for $K_y=14.7$.

This wiggler is now installed in the storage ring, and experiments are beginning to measure the degree of circular polarization using a magnetic Compton scattering experiment. The experiment is being performed at 47 keV, 65 keV, 86 keV, 115 keV and 150 keV. At each energy, measurements were done for the following K_x values : 1.3, 1.0, 0.8 and 0 (i.e., no horizontal magnetic field applied). The exception was at 86 keV, where the polarity was varied. Helicity switching was observed as expected.